# Toward Versatile Sr$_2$FeMoO$_6$-Based Spintronics by Exploiting Nanoscale Defects

Minnamari Saloaro,[*,†] Martin Hoffmann,[‡,§,∥] Waheed A. Adeagbo,[§] Sari Granroth,[⊥] Hakan Deniz,[∥] Heikki Palonen,[†] Hannu Huhtinen,[†] Sayani Majumdar,[†,#] Pekka Laukkanen,[⊥] Wolfram Hergert,[§] Arthur Ernst,[∥] and Petriina Paturi[†]

[†]Wihuri Physical Laboratory, Department of Physics and Astronomy, University of Turku, Turku FI-20014, Finland
[‡]IFW Dresden, P.O. Box 27 01 16, D-01171 Dresden, Germany
[§]Institut für Physik, Martin Luther University Halle-Wittenberg, Von-Seckendorff-Platz 1, 06120 Halle, Germany
[∥]Max Planck Institute of Microstructure Physics, Weinberg 2, 06120 Halle, Germany
[⊥]Materials Research Laboratory, Department of Physics and Astronomy, University of Turku, Turku FI-20014, Finland
[#]NanoSpin, Department of Applied Physics, Aalto University School of Science, P.O. Box 15100, FI-00076 Aalto, Finland

**Ⓢ** *Supporting Information*
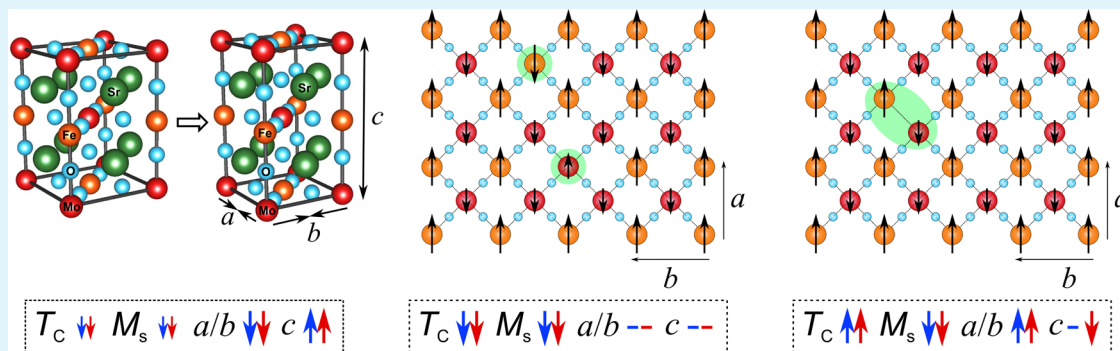
**ABSTRACT:** To actualize the high spintronic application potential of complex magnetic oxides, it is essential to fabricate these materials as thin films with the best possible magnetic and electrical properties. Sr$_2$FeMoO$_6$ is an outstanding candidate for such applications, but presently no thin film synthesis route, which would preserve the magnetic properties of bulk Sr$_2$FeMoO$_6$, is currently known. In order to address this problem, we present a comprehensive experimental and theoretical study where we link the magnetic and half metallic properties of Sr$_2$FeMoO$_6$ thin films to lattice strain, Fe—Mo antisite disorder and oxygen vacancies. We find the intrinsic effect of strain on the magnetic properties to be very small, but also that an increased strain will significantly stabilize the Sr$_2$FeMoO$_6$ lattice against the formation of antisite disorder and oxygen vacancies. These defects, on the other hand, are recognized to drastically influence the magnetism of Sr$_2$FeMoO$_6$ in a nonlinear manner. On the basis of the findings, we propose strain manipulation and reductive annealing as optimization pathways for improving the spintronic functionality of Sr$_2$FeMoO$_6$.

**KEYWORDS:** spintronics, SFMO, nanoscale defects, strain, oxygen vacancy, antisite disorder, first-principles, magnetic properties

## 1. INTRODUCTION

Complex magnetic oxides have drawn great scientific interest due to their high potential for novel spintronics. Especially, the magnetic and resistive properties of the double perovskite Sr$_2$FeMoO$_6$ (SFMO) are excellent for spintronic and magneto-resitive applications. With the Curie temperature, $T_C$, of around 450 K, SFMO possesses a high spin polarization and a large intrinsic magnetoresistance even at room temperature.[1] These characteristics make SFMO a potentially better candidate than widely used half-metallic La$_{0.67}$Sr$_{0.33}$MnO$_3$.[2] However, in order to use SFMO in multilayer devices, it is essential to avoid deterioration of the magnetic and electrical properties of films in comparison with the bulk material, which is extremely

challenging. The literature has so far identified that substrate induced strain, antisite disorder (ASD), and the appearance of oxygen vacancies (V$_O$) are the most prominent mechanisms whose interplay determines the degradation of the film properties.[3−8] Nevertheless, a comprehensive understanding of their individual and collective role is challenging and still missing. The current investigation provides significant experimental data and a theoretical analysis to clarify the role of

TH-2016-34

different mechanisms behind the weakened magnetic properties of $Sr_2FeMoO_6$ thin films compared to polycrystalline samples.

Several properties in thin films might be influenced by the substrate induced strain, which can be varied by changing the film thickness or by using substrates with different lattice mismatches. In Manganite thin films, the strain induces magnetic anisotropy and changes both resistivity and magnetic properties.[9,10] Strain has also been seen to affect the surface morphology by increasing the surface roughness and to weaken the magnetic properties of the SFMO thin films.[7,11,12]

In the perfect SFMO structure (Figure 1a), the Mo and Fe ions are in alternating rock salt type order. The magnetic
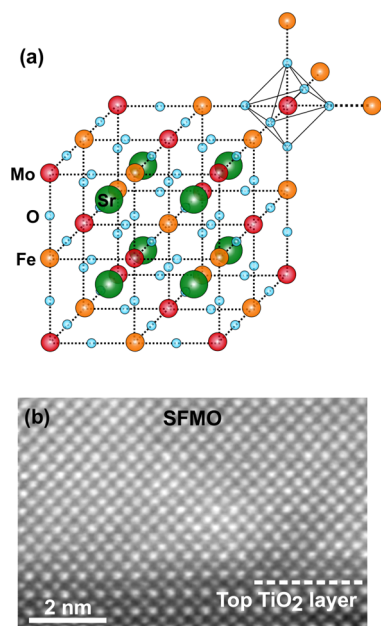


**Figure 1.** (a) Schematic picture of the cubic crystal structure of SFMO. (b) The HAADF-STEM image of the SFMO/STO interface, where the dashed line indicates the topmost $TiO_2$ layer.

ground state is usually considered as a ferrimagnetic collinear state with parallel Fe moments, which are antiparallel to Mo moments. The perfect structure is easily varied by ASD, which causes the exchange of positions of the Fe and Mo ions. The ASD is already known to reduce the saturation magnetization, since the observed antiferromagnetic (AFM) superexchange of the antisite $Fe—O—Fe_{Mo}$ bonds leads to a larger component of antiparallel aligned magnetic moments.[13–17] At concentrations below 15% of ASD, a decrease in $T_C$ with increasing amount of ASD has been reported.[6,14–16] However, at higher degrees of disorder, the AFM character of the Fe—O—Fe bonds dominates the magnetic order and AFM ground state is observed.[13]

Oxygen vacancies, $V_O$, are rather common defects in SFMO, since the fabrication of SFMO is very sensitive to the applied atmosphere. For example, extra oxygen in the fabrication process often leads to impurity phases.[7,18] The literature about the polycrystalline SFMO at hand has so far presented strong evidence, also supported by several theoretical studies, that an increasing number of oxygen vacancies reduces the saturation magnetization, $M_s$, of SFMO.[6,8,16,19–22] However, the number of reports about the effect of oxygen vacancies on the Curie temperature of SFMO is more limited. Our previous theoretical study suggests higher $T_C$ in oxygen deficient SFMO.[16] On the

contrary, a decreased $T_C$ has been experimentally observed in oxygen deficient polycrystalline SFMO, in which the effects of other structural defects like ASD were not completely ruled out.[22] Thus, the role of oxygen vacancies in SFMO thin films is still not clear, despite the various experimental and theoretical studies about the polycrystalline SFMO.

In this work, we compare two sample types of SFMO, thin films made with pulsed laser deposition (PLD) on $SrTiO_3$ (001) (STO) single crystal substrates and the polycrystalline bulk, i.e., the target used in the film deposition. The fabrication and the structural quality of the films and polycrystalline material have been reported earlier.[23–25] These previous results show that no impurity phases have been observed in our samples within the detection limit of X-ray diffraction (XRD). The high and uniform quality of the films used in these investigations were confirmed with the X-ray diffraction (XRD) and transmission electron microscopy (TEM) measurements, the details of which are given in the Supporting Information (SI). The experimental results are complemented by the first-principles calculations.

## 2. RESULTS AND DISCUSSION

The temperature and the field dependences of the magnetization were measured from both sample types to determine the $T_C$ as a minimum of the temperature derivative and $M_s$. The $T_C$ of the standard 160 nm thick SFMO film was found to be around 320 K, whereas the $T_C$ of the polycrystalline bulk material is 23% higher, around 400 K. However, the $M_s$ of the film is around 2.6 $\mu_B$/f.u., which is 33% higher than in the bulk sample ($M_s = 2$ $\mu_B$/f.u.) and clearly lower than the theoretical ideal value of 4 $\mu_B$/f.u.. The reduction of $M_s$ from the theoretical value and the lowering of the $T_C$ in the thin film are significant. Especially, the decreased $T_C$ is less favorable for possible applications. Hence, the systematic experiments to separately investigate the deteriorating mechanisms will pave the way to improve $T_C$ of the thin films.

The effect of strain was studied by varying the film thickness from 50 to 160 nm. Films with different thicknesses were used instead of growing films on different substrates to avoid the effect of substrate induced interface defects. This is especially important in SFMO thin films, because previous investigations have shown that the interface defects dominate their magnetic properties and that the formation of these defects is highly dependent on the substrate material.[26] A coherent film/substrate interface and a low amount of interface defects were also confirmed with TEM studies (Figure 1b). Therefore, it is not expected that interface defects contribute notably to the observed differences in the physical properties of the films used in this work.

The substrate induced in-plane, $\varepsilon_a$, and out-of-plane, $\varepsilon_c$, strains were determined from the $a$ and $c$ parameters obtained from the XRD measurements with respect to the lattice parameters of bulk SFMO ($a_b = 5.575$ Å, $c_b = 7.893$ Å).[26,27] A compressive in-plane strain was observed in all the films as expected from the lattice mismatch of $-1.05\%$ between the STO substrate and SFMO. Such an in-plane compression often results in an increase of the out-of-plane lattice constant. A tensile strain $\varepsilon_c$ was indeed observed experimentally. The magnitude of both strain values reduces monotonously with increasing film thickness. Up to 120 nm, the in-plane strain decreased from $-0.79\%$ to $-0.31\%$ and remained almost constant in the two thickest films. This implies that the SFMO
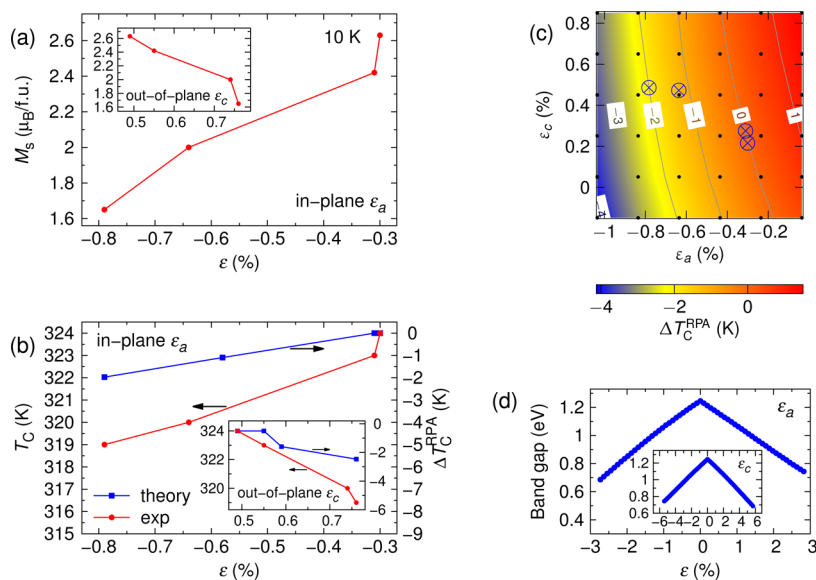
**Figure 2.** (a) $M_s$ of the SFMO films versus in-plane and out-of-plane strain. (b) The experimental $T_C$ and (right-hand scale) the theoretical $\Delta T_C$ with respect to the theoretical value corresponding to the least strained film versus in-plane and out-of-plane strain. (c) $\Delta T_C$ in a contour plot in a range near to the experiment. The crossed circles mark the four experimental data points. (d) Theoretical variation of the majority spin band gap versus in-plane and out-of-plane strain. The $c$ direction was always relaxed.
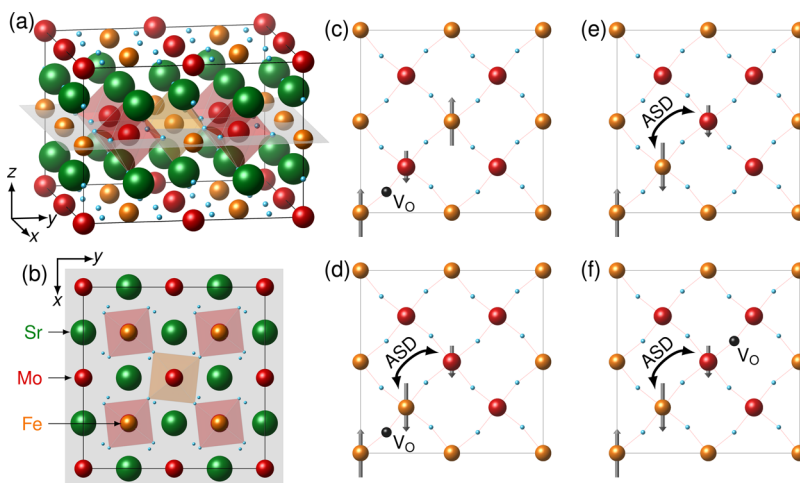


**Figure 3.** Lattice structure of SFMO in a supercell of 8 f.u. used for the bulk defect calculations. The atoms are shown as colored balls (Sr, green; Fe, orange; Mo, red; O, blue): (a) Sideview. The gray plane indicates the plane where defects were included. (b) Topview. (c)−(f) Sketch of the simulated defect configurations in the supercell. The black arrows visualize a swap of Fe and Mo (ASD). The black ball shows a vacancy. The gray arrows symbolize the relative orientation and the size of the magnetic moments. They are not particularly in the $x−y$ plane.

films are relaxed at a thickness between 80 and 120 nm, which agrees with the results of Fix et al.[28]

A monotonic increase of $M_s$ of 1 $\mu_B$/f.u. was observed with decreasing in-plane strain, i.e., increasing layer thickness (Figure 2a). The calculated magnetic moments were almost independent of the variations in the lattice parameters, and the changes were smaller than 1%. The experimental values of the Curie temperature increase monotonously with decreasing in-plane strain $\varepsilon_a$ in good qualitative agreement with calculated Curie temperatures (Figure 2b). However, the increase of $T_C$ in the experimentally accessible range remained in the range of few kelvin. When the experimental curves are extrapolated toward zero strain, an additional estimated increase of 1−2 K in $T_C$ and around 0.4 in $M_s$ is achieved. However, this is still insignificant when compared to the 80 K larger $T_C$ of the polycrystalline bulk material.

Calculations for a larger range of strain show that the Curie temperature varies only by few kelvin and depends mainly on the in-plane strain (Figure 2c). We predict that also the majority spin-band determining the half-metallic character of SFMO is preserved for these strains (Figure 2d). Thus, the theoretical and experimental results clearly prove that the experimentally observed strain alone cannot explain the deteriorated properties in thin films.

Nevertheless, the strain might have a stronger indirect influence on the magnetic properties of the film via altered formation probabilities of the possible defects. Previous investigations have suggested that the changes in the magnetic properties of SFMO are likely connected to the amount of ASD and oxygen vacancies,[6,16,29−31] but no information about their appearance probability in different types of samples have been provided. A conclusive step toward the estimation of the

likelihood of such defects by theoretical means is the calculation of formation energies, $E_{form}$, as a function of the oxygen chemical potential, $\mu_O$, for different defects (Figure 3). When we compared $E_{form}$ of several defect combinations calculated either at the relaxed SFMO lattice constant or compressed to the experimental lattice constant of STO, the latter always yielded a higher $E_{form}$, i.e., 40% and 13% higher for ASD or $V_O$, respectively (Table 1). This indicates a reduced probability of forming a defect in strained thin films.

**Table 1. Formation Energies, $E_{form}$, at O-Rich Conditions and the Majority Spin Band Gaps, $\Delta^{\uparrow}$, of the Defect Configurations Shown in Figure 3 for SFMO Bulk with Respect to the Defect-Free Sample[a]**

|  | configurations | $E_{form}$ [eV] | | $\Delta^{\uparrow}$ [eV] |
|---|---|---|---|---|
|  |  | $a_{SFMO}$ | $a_{STO}$ | $a_{SFMO}$ |
| (a),(b) | defect-free | 0.0000 | 0.61144 | 1.20 |
| (c) | $V_O$ | 4.6539 | 5.16068 | 1.10 |
| (d) | ASD | 0.7712 | 1.37307 | 0.00 |
| (e) | ASD + $V_O$(Fe—O—Fe$_{Mo}$) | 4.5922 | 5.29722 | 0.00 |
| (f) | ASD + $V_O$(Mo—O—Mo$_{Fe}$) | 6.0269 | 6.79441 | 0.00 |

[a]The formation energies are compared for two different in-plane lattice constants (see text).

The same tendency was experimentally observed when comparing the films and the polycrystalline bulk samples. The ASD of the films were obtained from the intensity ratio of the (101) and (404) peaks and for the bulk material with the Rietveld refinement using the Maud program.[26,32] These disorder values for the film and bulk are independent of each other, because the material transferred from the target to the film is fully vaporized in the PLD process before recrystallization. The ASD of the polycrystalline material was found to be around 28%, which is at least twice as large as the $12 \pm 3\%$ of ASD in the films. Thus, the higher amount of ASD in the polycrystalline material is in good agreement with the $E_{form}$ analysis and could also explain the reduced $M_s$ of the bulk sample.

Alternatively, according to the earlier theoretical results and previous experiments,[14−16] $T_C$ and $M_s$ have a decreasing tendency at least up to 15% of ASD. However, the observed ASD level in the target is far above this range. For larger amounts of ASD, Sanchez et al.[13] have found indications of an ordered antiferrromagnetic structure with higher ordering temperature of 770 K. This fact allows us to expect that the critical temperature might increase for an ASD concentration larger than 15%. This assumption is supported by the strong AFM coupling that we observed between the original Fe sites and the antisite Fe at Mo site (see the SI). This might dominate the magnetic ground state for higher amounts of ASD. However, it was not possible to reliably determine the transition temperature for more than 15% of ASD in the theoretical calculations including the effective medium description.[16] Therefore, we modeled a periodical arrangement of 25% of ASD (one inverted Fe—O—Mo bond per 4 f.u. of SFMO) in a supercell approach. The calculation yielded a high magnetic transition temperature of 740 K due to the strong AFM coupling between Fe—O—Fe (see the SI). These results suggest that the decreasing tendency of $T_C$ in the low concentration limit of ASD turns to an increasing one for higher disorder concentration. This corresponds well with the

measured $T_C$ values, which were lower in the film with $12 \pm 3\%$ of ASD and higher in the polycrystalline bulk material with 28% of ASD. Even though our findings would imply that the $T_C$ could be increased more with high ASD concentrations, the magnetic ground state, the saturation magnetization, and the half metallicity of the films deteriorate. The latter could be observed from previous experiments[33] and in our density of states (DOS) calculations including ASD, where an additional state from Mo at the Fe site arises at the Fermi energy. Therefore, even higher B-site ordering is still desired when these films are considered for applications, although we already observed a strong 50% reduction of ASD by growing the films with PLD.

In addition to the ASD, a lower amount of oxygen vacancies, $V_O$, is expected in the films compared to the polycrystalline bulk from the $E_{form}$ calculations. According to our previous theoretical investigations,[16] a greater number of oxygen vacancies increases $T_C$ and decreases $M_s$. This explains the large difference in $T_C$ between the target and the film. In order to experimentally investigate the effect of oxygen vacancies in SFMO, a thin film corresponding to the one used in the ASD studies (pristine) was annealed in ultra high vacuum conditions (annealed). The carefully implemented ex situ post annealing was used to vary the oxygen stoichiometry in the sample, because smaller amount of structural modifications is observed when compared to the films grown with different deposition atmospheres (see the SI).[23] Hence, the vacuum annealing enables one to minimize the contribution of other structural defects better than varying the deposition atmosphere. The optimization of the vacuum annealing parameters is presented in the SI.

A change in the lattice parameters was experimentally observed after the vacuum annealing. The $a$ parameter was increased by 0.3%, while the $c$ parameter was decreased by 0.1%. An increase in the $a$ parameter has also been observed in oxygen deficient polycrystalline SFMO, while the results for the $c$ parameter has been inconsistent.[20,22] On the contrary, a previous theoretical study has suggested a decrease in both $a$ and $c$ parameters with the increasing amount of oxygen vacancies.[34] The increasing unit cell volume is generally associated with the formation of oxygen vacancies in complex metal oxides, since the cation−cation bond is longer than the cation−oxygen−cation bond. Due to the charge compensation, the oxidation state of the cation is reduced, which also increases the ionic radii of the cations. Moreover, the changes in the number of ASD before and after vacuum annealing are within the normal variation of around 3 percentage points. Within the observed ASD range of the films, the changes in $T_C$ due to the normal variation cannot explain the differences between the pristine and annealed films. Thus, we expect that the observed 20 K increase in $T_C$ and a 0.2 $\mu_B$/f.u. decrease in $M_s$ were caused mainly by oxygen vacancies (Figure 4a). These variations correspond already to a 6% change in both quantities in regard to the pristine sample.

In order to further investigate the changes in the oxygen vacancy concentration caused by the vacuum annealing, bulk sensitive hard X-ray photoelectron spectroscopy (HAXPES) measurements were carried out. The experimental valence band spectra, which provide information about the total DOS distribution, were compared qualitatively with the calculated density of states for defect-free SFMO, SFMO including ASD and SFMO with $V_O$ (Figure 4b,c). The structures at small binding energies (between 0 and 2 eV) are attributed to the Fe
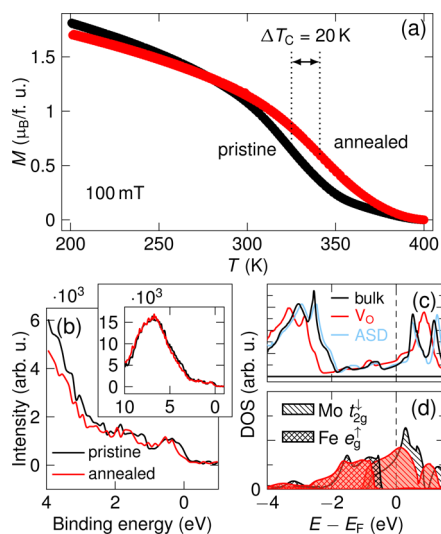
**Figure 4.** (a) Magnetization curves in 100 mT field for the pristine and vacuum annealed SFMO films. (b) Valence band photoemission spectra of the pristine (black) and annealed (red) samples. The inset shows a larger energy range. (c) Theoretical DOS for defect-free SFMO, 10 at. % ASD or 8 at. % $V_O$. The dashed line indicates the Fermi energy, $E_F$. (d) The partial DOS for the relevant Fe $e_g^\uparrow$ and Mo $t_{2g}^\downarrow$ states are compared with the bulk (black patterns) and $V_O$ calculations (red patterns).

$3d$ and Mo $4d$ states. The experimental results at low binding energies yield a shift of these features toward higher binding energies when the valence band spectrum of the annealed film is compared with the one of the pristine film (compare red with black line in Figure 4b). The increasing binding energies correspond to a downward shift of the electronic states in the DOS or an increase of the Fermi energy, $E_F$. Such a shift is only observed for the DOS of oxygen-deficient SFMO, whereas ASD does not change the DOS significantly with respect to bulk SFMO (Figure 4c). The oxygen vacancies and the additional electrons change the oxidation states of the Fe and Mo ions and increase $E_F$. In particular, the position of the Fe $3d$ and Mo $4d$ states close to $E_F$ is changed (Figure 4d).

In addition to the changes observed in the valence band spectra, the binding energies of Fe $2p$, Mo $3d$, Sr $3d$, and O $1s$ states are also increased (approximately +0.2 eV). Similar shifts

in the Sr $3d$ and O $1s$ spectra of the $SrTiO_3$ and $SrFeO_x$ have been observed with increasing amount of oxygen vacancies.[35,36] Hence, the HAXPES results support the assumption that the vacuum annealing leads to a higher oxygen deficiency in SFMO thin films. These experimental results are in good agreement with our previous theoretical results[16] and confirm that the $T_C$ of SFMO can be improved by increasing the amount of oxygen vacancies. Unlike the ASD, the increasing amount of oxygen vacancies do not even deteriorate the spin polarization essential for applications. This preserved half metallicity of oxygen deficient SFMO is also supported by other theoretical studies.[34,37,38]

To summarize our theoretical and experimental approaches, the change of the magnetic properties of SFMO is a complex issue, which is caused by a combination of nanoscale mechanisms. The three most probable factors are strain, ASD, and oxygen vacancies, which are schematically crystallized in Figure 5. Even though the effect of increasing compressive strain itself is insignificant, the formation energy calculations suggest that the formation of oxygen vacancies and ASD is less probable in compressively strained films. Thus, the substrate induced strain cannot be ignored in the context of defect variation. The result that an increasing strain could stabilize the SFMO lattice against the formation of ASD and oxygen vacancies is significant and could also be extrapolated for other perovskite materials.

As summarized in Figure 5, the small compression from the substrate decreases the in-plane $a/b$ parameter, which leads to an elongation of the out-of-plane $c$ parameter. Alternatively, the transposed Fe/Mo ions have small enough difference in their ionic radii that no changes can be observed in the lattice parameters, whereas the absence of oxygen ions causes an increase in the $a/b$ parameter. Even though the magnetic properties of SFMO are only slightly influenced by the strain, the role of ASD and oxygen vacancies is extremely significant. The Fe ions are AFM coupled with a large coupling constant to the Fe ion in the antisite position, which reduces the saturation magnetization and the Curie temperature, until at higher ASD concentrations, the strong AFM coupling leads to an increase in $T_C$. In addition, the half metallic character is deteriorated due the additional states of antisite Mo at the Fermi energy. The formation of the oxygen vacancy results in enhanced antiferromagnetic coupling between Fe and Mo. This
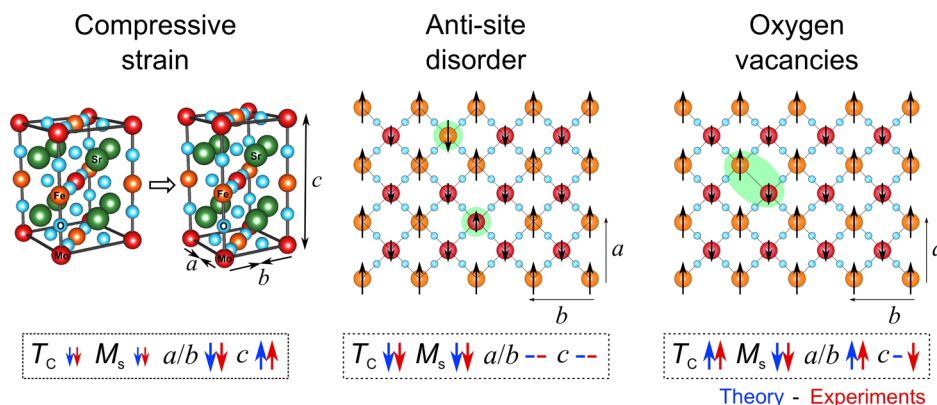


**Figure 5.** A schematic picture of the changes in SFMO thin films caused by compressive strain, antisite disorder, and oxygen vacancies. The structural modifications due to these defects are illustrated at the top and the changes in the main magnetic and structural properties from the experiments (red) and theoretical calculations (blue) at the bottom. The arrows imply the direction of change in the defect concentration range of the films and the lines represent constancy.

strengthens the ferromagnetic coupling between the Fe ions and leads to the observed increase in the Curie temperature.[16] This also leads to a slightly reduced saturation magnetization, but the half metallic feature remains preserved. Altogether, the ASD concentrations larger than 15% and the increasing amount of oxygen vacancies both increase the $T_C$ and decrease the $M_s$ of SFMO. Therefore, the 80 K higher $T_C$ and the 0.6 $\mu_B$/f.u. smaller $M_s$ of the polycrystalline bulk SFMO can be explained as a combined effect of large ASD concentration and higher amount of oxygen vacancies.

## 3. CONCLUSIONS

Our results show that the first priority toward SFMO films for applications is to further reduce the amount of ASD, which would improve all important properties. In addition, we conclusively show that the Curie temperature of SFMO can be increased without deteriorating the half metallicity by increasing the number of oxygen vacancies. Therefore, the role of oxygen vacancy engineering is extremely important and should not be underestimated in the future optimization processes. Since the ASD and oxygen vacancies are important factors in other perovskite materials that have been suggested for spintronic applications, it is expected that the strain engineering and vacuum annealing will be important concepts to improve the properties of these materials in general.

## 4. EXPERIMENTAL SECTION

**4.1. Thin Film Fabrication.** The films were grown with pulsed laser deposition (PLD) using a XeCl excimer laser at $\lambda = 308$ nm. The deposition temperature, $T_d$, was 1050 °C and the films were made in 9 Pa pressure Ar atmosphere. The laser repetition rate was 5 Hz. The details of the target preparation with the sol−gel method are reported in refs 39 and 40 and the film deposition in refs 23 and 25. Also, ex situ vacuum annealing at 650 °C in $10^{-9}$ mbar for 120 min was carried out with a standard 160 nm thick film.

**4.2. Structural Characterization.** X-ray diffraction (XRD) measurements were made with a Philips X'pert Pro MPD diffractometer in the Bragg−Brentano $\theta$−$2\theta$ configuration with Cu $K_\alpha$ radiation, incident beam X-ray mirror, and Schulz texture goniometer. Transmission electron microscopy (TEM) studies were made with TITAN 80−300 at the voltage of 300 kV. A probe-corrected scanning TEM using high-angle annular dark field imaging (HAADF) were carried out for a focused ion beam (FIB) lamella prepared from the 160 nm thick sample. The X-ray photoelectron spectroscopy spectra were obtained by synchrotron radiation excited hard X-ray photoelectron spectroscopy (HAXPES). The measurements were carried out at HIKE end-station of the KMC-1 beamline in BESSY II (Helmholz-Zentrum Berlin). The HAXPES spectra were measured with photon energy of 5000 eV at room temperature. The binding energy scale was calibrated using Au $4f_{7/2}$ core levels of a calibration sample.

**4.3. Magnetic Measurements.** A Quantum design MPMS SQUID magnetometer was used in the magnetic measurements. The zero field cooled (ZFC) and field cooled (FC) magnetization curves were measured in 100 mT and 500 mT for all the samples. The Curie temperatures of the SFMO films were defined from the 500 mT FC magnetization curves as a minimum of the temperature derivative. The hysteresis loops were measured between −0.5 and 0.5 T at 10, 100, 300, and 400 K. In all these measurements, the plane of the film was parallel to the external magnetic field. The dia- and paramagnetic effects from the substrate and the sample holder were subtracted from the measured data.

**4.4. First-Principles Calculations.** We used two methods based on density functional theory, the Green's function (GF) method HUTSEPOT[41,42] to obtain the magnetic properties, and the Vienna ab initio simulation package (VASP)[43,44] to determine the structural relaxations and the corresponding formation energies. To treat electron exchange and correlation, we chose in both methods the Perdew−Burke−Ernzerhof formulation of the generalized gradient approximation (GGA).[45] The $\vec{k}$ points were sampled according to the Monkhorst−Pack automatic generation scheme with special $\vec{k}$ point meshs large enough to ensure the proper convergence of the desired physical quantities. Both methods agreed well with the electronic structure obtained in the primitive unit cell.[16] The volume variation or the strain is simulated by changing stepwise the $a$ and $c$ lattice parameters of the defect-free primitive unit cell. Then, we determined the Curie temperature by means of the random-phase approximation (RPA).[46] The defect configurations were considered with VASP within a supercell consisting of $2 \times 2 \times 2$ tetragonal unit cells, in total with 80 atoms (Figure 3). More computational details are provided in the Supporting Information (SI).

**4.5. Formation Energy.** The method to calculate the charge free defect formation energy, $E_{form}$, for a particular defect type with VASP is the same as that used for $BaTiO_3$.[47] Therein, the total energy and the chemical potentials of possible vacancies are needed. We calculated the total energy of $V_O$, ASD, and possible combinations of both defects in the supercell. The necessary chemical potentials of oxygen, $\mu_O$, which represents the O-rich limit, was derived from the half of the total energy of an oxygen molecule alone in the volume of the supercell.

## ■ ASSOCIATED CONTENT

**Ⓢ Supporting Information**

The Supporting Information is available free of charge on the ACS Publications website at DOI: 10.1021/acsami.6b04132.

> Details of the structural and magnetic characterization of the SFMO films; XRD patterns, magnetization curves, and hysteresis loops (Figures S1 and S2); Thicknesses, lattice parameters, strains, Curie temperatures, and saturation magnetization values (Table S1); Optimization process of the ex situ vacuum annealing treatment; Computational details (Green's function method, VASP); and Magnetic exchange interactions for the three degradation mechanisms (PDF)

## ■ AUTHOR INFORMATION

**Corresponding Author**

*E-mail: minnamari.saloaro@utu.fi (M.S.).

**Notes**

The authors declare no competing financial interest.

## ■ ACKNOWLEDGMENTS

## ■ REFERENCES

(1) Kobayashi, K.-I.; Kimura, T.; Sawada, H.; Terakura, K.; Tokura, Y. Room-Temperature Magnetoresistance in an Oxide Material with an Ordered Double-Perovskite Structure. *Nature* **1998**, *395*, 677−680.

(2) Majumdar, S.; van Dijken, S. Pulsed Laser Deposition of $La_{1-x}Sr_xMnO_3$: Thin-Film Properties and Spintronic Applications. *J. Phys. D: Appl. Phys.* **2014**, *47*, 034010.

(3) Hauser, A. J.; Williams, R. E. A.; Genc, A.; Lucy, J. M.; Woodward, P. M.; Fraser, H. L.; Yang, F. Unlocking the Potential of Half-Metallic $Sr_2FeMoO_6$ Films Through Controlled Stoichiometry and Double-Perovskite Ordering. *Phys. Rev. B: Condens. Matter Mater. Phys.* **2011**, *83*, 014407.

(4) Meneghini, C.; Ray, S.; Liscio, F.; Bardelli, F.; Mobilio, S.; Sarma, D. D. Nature of "Disorder" in the Ordered Double Perovskite $Sr_2FeMoO_6$. *Phys. Rev. Lett.* **2009**, *103*, 046403.

(5) Erten, O.; Meetei, O. N.; Mukherjee, A.; Randeria, M.; Trivedi, N.; Woodward, P. Theory of Half-metallic Ferrimagnetism in Double Perovskites. *Phys. Rev. Lett.* **2011**, *107*, 257201.

(6) Ogale, A. S.; Ogale, S. B.; Ramesh, R.; Venkatesan, T. Octahedral Cation Site Disorder Effects on Magnetization in Double-Perovskite $Sr_2FeMoO_6$: Monte Carlo Simulation Study. *Appl. Phys. Lett.* **1999**, *75*, 537−539.

(7) Sánchez, D.; García-Hernández, M.; Auth, N.; Jakob, G. Structural, Magnetic, and Transport Properties of High-Quality Epitaxial $Sr_2FeMoO_6$ Thin Films Prepared by Pulsed Laser Deposition. *J. Appl. Phys.* **2004**, *96*, 2736−2742.

(8) Colis, S.; Stoeffler, D.; Meny, C.; Fix, T.; Leuvrey, C.; Pourroy, G.; Dinia, A.; Panissod, P. Structural Defects in $Sr_2FeMoO_6$ Double Perovskite: Experimental Versus Theoretical Approach. *J. Appl. Phys.* **2005**, *98*, 033905.

(9) Ranno, L.; Llobet, A.; Tiron, R.; Favre-Nicolin, E. Strain-Induced Magnetic Anisotropy in Epitaxial Manganite Films. *Appl. Surf. Sci.* **2002**, *188*, 170−175.

(10) Zhang, P. X.; Zhang, H.; Cha, L. M.; Habermeier, H.-U. Tailoring the Physical Properties of Manganite Thin Films by Tuning the Epitaxial Strain. *Phys. B* **2003**, *327*, 257−261.

(11) Boucher, R. $Sr_2FeMoO_{6+x}$: Film Structure Dependence Upon Substrate Type and Film Thickness. *J. Phys. Chem. Solids* **2005**, *66*, 1020−1024.

(12) Jalili, H.; Heinig, N. F.; Leung, K. T. Growth Evolution of Laser-Ablated $Sr_2FeMoO_6$ Nanostructured Films: Effects of Substrate-Induced Strain on the Surface Morphology and Film Quality. *J. Chem. Phys.* **2010**, *132*, 204701.

(13) Sanchez, D.; Alonso, J. A.; Garcia-Hernandez, M.; Martinez-Lope, M. J.; Martinez, J. L.; Mellergård, A. Origin of Neutron Magnetic Scattering in Antisite-Disordered $Sr_2FeMoO_6$ Double Perovskites. *Phys. Rev. B: Condens. Matter Mater. Phys.* **2002**, *65*, 104426.

(14) Moritomo, Y.; Shimamoto, N.; Xu, S.; Machida, A.; Nishibori, E.; Takata, M.; Sakata, M.; Nakamura, A.; Oritomo, Y. M.; Himamoto, N. S.; Sheng, X. U.; Achida, A. M.; Ishibori, E. N.; Akata, M. T. Effects of B-Site Disorder in $Sr_2FeMoO_6$ with Double Perovskite Structure. *Jpn. J. Appl. Phys.* **2001**, *40*, L672−L674.

(15) Huang, Y.; Karppinen, M.; Yamauchi, H.; Goodenough, J. Systematic Studies on Effects of Cationic Ordering on Structural and Magnetic Properties in $Sr_2FeMoO_6$. *Phys. Rev. B: Condens. Matter Mater. Phys.* **2006**, *73*, 104408.

(16) Hoffmann, M.; Antonov, V. N.; Bekenov, L. V.; Kokko, K.; Hergert, W.; Ernst, A. Impact of Lattice Defects and Electron Correlations on the Magnetic Properties of $Sr_2FeMoO_6$. *ArXiv:1504.02629* **2016**.

(17) Solovyev, I. V. Electronic Structure and Stability of the Ferrimagnetic Ordering in Double Perovskites. *Phys. Rev. B: Condens. Matter Mater. Phys.* **2002**, *65*, 144446.

(18) Santiso, J.; Figueras, A.; Fraxedas, J. Thin Films of $Sr_2FeMoO_6$ Grown by Pulsed Laser Deposition: Preparation and Characterization. *Surf. Interface Anal.* **2002**, *33*, 676−680.

(19) Kircheisen, R.; Töpfer, J. Nonstoichiometry, Point Defects and Magnetic Properties in $Sr_2FeMoO_{6-\delta}$ Double Perovskites. *J. Solid State Chem.* **2012**, *185*, 76−81.

(20) Töpfer, J.; Kircheisen, R.; Barth, S. Nonstoichiometry, Point Defects, and Magnetoresitance of $Sr_2FeMoO_{6-\delta}$. *J. Appl. Phys.* **2009**, *105*, 07D712.

(21) Taylor, D. D.; Schreiber, N. J.; Brown, C. M.; Arevalo-Lopez, A. M.; Rodriguez, E. E. Stabilization of Cubic $Sr_2FeMoO_6$ Through Topochemical Reduction. *Chem. Commun.* **2015**, *51*, 12201−12204.

(22) Zhang, Q.; Xu, Z. F.; Wang, L. F.; Gao, S. H.; Yuan, S. J. Structural and Electronic Properties Driven by Oxygen Vacancy in $Sr_2FeMoO_6$ Double Perovskite. *J. Alloys Compd.* **2015**, *649*, 1151−1155.

(23) Paturi, P.; Metsänoja, M.; Huhtinen, H. Optimization of Deposition Temperature and Atmosphere for Pulsed Laser Deposited $Sr_2FeMoO_6$ Thin Films. *Thin Solid Films* **2011**, *519*, 8047−8052.

(24) Saloaro, M.; Majumdar, S.; Huhtinen, H.; Paturi, P. Absence of Traditional Magnetoresistivity Mechanisms in $Sr_2FeMoO_6$ Thin Films Grown on $SrTiO_3$, MgO and $NdGaO_3$ Substrates. *J. Phys.: Condens. Matter* **2012**, *24*, 366003.

(25) Suominen, T.; Raittila, J.; Paturi, P. Pure and Fully Texturized $Sr_2FeMoO_6$ Thin Films Prepared by Pulsed Laser Deposition from Target Made with Citrate-Gel Method. *Thin Solid Films* **2009**, *517*, 5793−5797.

(26) Saloaro, M.; Deniz, H.; Huhtinen, H.; Palonen, H.; Majumdar, S.; Paturi, P. The Predominance of Substrate Induced Defects in Magnetic Properties of $Sr_2FeMoO_6$ Thin Films. *J. Phys.: Condens. Matter* **2015**, *27*, 386001.

(27) Nakamura, S.; Oikawa, K. Precise Structure Analysis Consistent with Mössbauer Quadrupole Effect: A Case of the Ordered Double Perovskites $Sr_2FeMO_6$ (M = Mo and Re). *J. Phys. Soc. Jpn.* **2003**, *72*, 3123−3127.

(28) Fix, T.; Stoeffler, D.; Colis, S.; Ulhaq, C.; Versini, G.; Vola, J. P.; Huber, F.; Dinia, A. Effects of Strain Relaxation on the Electronic Properties of Epitaxial $Sr_2FeMoO_6$ Grown by Pulsed Laser Deposition on $SrTiO_3$ (001). *J. Appl. Phys.* **2005**, *98*, 023712.

(29) Borges, R. P.; Lhostis, S.; Bari, M. A.; Versluijs, J. J.; Lunney, J. G.; Coey, J. M. D.; Besse, M.; Contour, J.-P. Thin Films of the Double Perovskite $Sr_2FeMoO_6$ Deposited by Pulsed Laser Deposition. *Thin Solid Films* **2003**, *429*, 5−12.

(30) Kumar, D.; Kaur, D. Substrate-Dependent Structural and Magnetic Properties of $Sr_2FeMoO_6$ Nanostructrured Double Perovskite Thin Films. *Phys. B* **2010**, *405*, 3259−3266.

(31) Singh, V. N.; Majumdar, P. Antisite Domains in Double Perovskite Ferromagnets: Impact on Magnetotransport and Half-Metallicity. *Europhys. Lett.* **2011**, *94*, 47004.

(32) Lutterotti, L. Material Analysis Using Diffraction 2.33 [computer program]. http://maud.radiographema.com, 1997−2011; Accessed: 2015-05-07.

(33) Panguluri, R. P.; Xu, S.; Moritomo, Y.; Solovyev, I. V.; Nadgorny, B. Disorder Effects in Half-Metallic $Sr_2FeMoO_6$ Single Crystals. *Appl. Phys. Lett.* **2009**, *94*, 012501.

(34) Wu, H.; Ma, Y.; Qian, Y.; Kan, E.; Lu, R.; Liu, Y.; Tan, W.; Xiao, C.; Deng, K. The Effect of Oxygen Vacancy on the Half-Metallic Nature of Double Perovskite $Sr_2FeMoO_6$: A Theoretical Study. *Solid State Commun.* **2014**, *177*, 57−60.

(35) Galakhov, V. R.; Kurmaev, E. Z.; Kuepper, K.; Neumann, M.; McLeod, J. A.; Moewes, A.; Leonidov, I. A.; Kozhenikov, V. L. Valence Band Structure and X-ray Spectra of Oxygen-Deficient Ferrites SrFeO. *J. Phys. Chem. C* **2010**, *114*, 5154−5159.

(36) Tan, H.; Zhao, Z.; Zhu, W.; Coker, E. N.; Li, B.; Zheng, M.; Yu, W.; Fan, H.; Sun, Z. Oxygen Vacancy Enhanced Photocatalytic Activity of Perovskite $SrTiO_3$. *ACS Appl. Mater. Interfaces* **2014**, *6*, 19184−19190.

(37) Stoeffler, D.; Colis, S. Ab Initio Study of the Electronic Structure of $Sr_2FeMoO_6$ Double Perovskites Presenting Oxygen Vacancies or/ and Antisite Imperfections. *Mater. Sci. Eng., B* **2006**, *126*, 133−138.

(38) Stoeffler, D.; Colis, S. Ab Initio Investigation of the Electonic Structure of $Sr_2FeMoO_6$ Double Perovskites Presenting Imperfections. *J. Magn. Magn. Mater.* **2005**, *290−291*, 400−404.

(39) Raittila, J.; Salminen, T.; Suominen, T.; Schlesier, K.; Paturi, P. Nanocrystalline $Sr_2FeMoO_6$ Prepared by Citrate-Gel Method. *J. Phys. Chem. Solids* **2006**, *67*, 1712−1718.

(40) Suominen, T.; Raittila, J.; Salminen, T.; Schlesier, K.; Linden, J.; Paturi, P. Magnetic Properties of Fine $Sr_2FeMoO_6$ Particles: Superparamagnetism. *J. Magn. Magn. Mater.* **2007**, *309*, 278−284.

(41) Ernst, A. *Multiple-Scattering Theory: New Developments and Applications*; Martin- Luther-Universität: Halle-Wittenberg, 2007.

(42) Lüders, M.; Ernst, A.; Temmerman, W. M.; Szotek, Z.; Durham, P. J. Ab Initio Angle-Resolved Photoemission in Multiple-Scattering Formulation. *J. Phys.: Condens. Matter* **2001**, *13*, 8587−8606.

(43) Kresse, G.; Hafner, J. Ab Initio Molecular Dynamics for Liquid Metals. *Phys. Rev. B: Condens. Matter Mater. Phys.* **1993**, *47*, 558−561.

(44) Kresse, G.; Furthmüller, J. Efficiency of Ab-Initio Total Energy Calculations for Metals and Semiconductors Using a Plane-Wave Basis Set. *Comput. Mater. Sci.* **1996**, *6*, 15−50.

(45) Perdew, J. P.; Burke, K.; Ernzerhof, M. Generalized Gradient Approximation Made Simple. *Phys. Rev. Lett.* **1996**, *77*, 3865−3868.

(46) Tiablikov, S. *Methods in the Quantum Theory of Magnetism*; Springer: New York, 1967/2013.

(47) Nayak, S. K.; Langhammer, H. T.; Adeagbo, W. A.; Hergert, W.; Müller, T.; Böttcher, R. Chromium Point Defects in Hexagonal $BaTiO_3$: A Comparative Study of First-Principles Calculations and Experiments. *Phys. Rev. B: Condens. Matter Mater. Phys.* **2015**, *91*, 155105.